GPS-derived strain in northwestern California: Termination of the San Andreas fault system and convergence of the Sierra Nevada–Great Valley block contribute to southern Cascadia forearc contraction

Todd B. Williams [a,1], Harvey M. Kelsey [b,*], Jeffrey T. Freymueller [c,2]

[a] UNAVCO, Inc., Plate Boundary Observatory, 1440 Regatta Blvd. Richmond, CA 94804, United States
[b] Department of Geology, Humboldt State University, Arcata, CA 95521, United States
[c] Geophysical Institute University of Alaska, Fairbanks, AK 99775, United States

Abstract

GPS-derived velocities (1993–2002) in northwestern California show that processes other than subduction are in part accountable for observed upper-plate contraction north of the Mendocino triple junction (MTJ) region. After removing the component of elastic strain accumulation due to the Cascadia subduction zone from the station velocities, two additional processes account for accumulated strain in northern California. The first is the westward convergence of the Sierra Nevada–Great Valley (SNGV) block toward the coast and the second is the north–northwest impingement of the San Andreas fault system from the south on the northern California coastal region in the vicinity of Humboldt Bay. Sierra Nevada–Great Valley block motion is northwest toward the coast, convergent with the more northerly, north–northwest San Andreas transform fault-parallel motion. In addition to the westward-converging Sierra Nevada–Great Valley block, San Andreas transform-parallel shortening also occurs in the Humboldt Bay region. Approximately 22 mm/yr of distributed Pacific–SNGV motion is observed inland of Cape Mendocino across the northern projections of the Maacama and Bartlett Springs fault zones but station velocities decrease rapidly north of Cape Mendocino. The resultant 6–10 mm/yr of San Andreas fault-parallel shortening occurs above the southern edge of the subducted Gorda plate and at the latitude of Humboldt Bay. Part of the San Andreas fault-parallel shortening may be due to the viscous coupling of the southern edge of the Gorda plate to overlying North American plate. We conclude that significant portions of the upper-plate contraction observed north of the MTJ region are not solely a result of subduction of the Gorda plate but also a consequence of impingement of the western edge of the Sierra Nevada–Great Valley block and growth of the northernmost segments of the San Andreas fault system.
© 2005 Elsevier B.V. All rights reserved.

Keywords: GPS geodesy; Cascadia subduction zone; Sierra Nevada–Great Valley block; San Andreas fault zone

* Corresponding author. Fax: +1 707 826 5241.
E-mail addresses: williams@unavco.org (T.B. Williams),
hmk1@humboldt.edu (H.M. Kelsey), jeff@giseis.alaska.edu
(J.T. Freymueller).
[1] Fax: +1 510 215 8105.
[2] Fax: +1 907 474 5618.

1. Introduction

Despite evidence for late Quaternary slip on active upper plate faults at the southern Cascadia margin (Kelsey and Carver, 1988; Clarke and Carver, 1992), only a few studies have attempted to measure present-

day deformation rates in this region (Lisowski et al., 1991; Snay and Matsikari, 1991; Murray et al., 1996; Murray and Lisowski, 2000). The purpose of this study is to provide, through repeated periodic Global Positioning System (GPS) surveys, an image of recent deformation (1993–2002) occurring near the Mendocino triple junction (MTJ), the southern Cascadia subduction zone (CSZ), and the northern end of the San Andreas fault (SAF) system, a region encompassed within the Mendocino deformation zone (MDZ; Fig. 1). We use contemporary GPS velocities to characterize the nature of interaction of Pacific–North America (P–NA) plate boundary deformation with the southern CSZ, and the pattern of distributed deformation of the northern California P–NA plate boundary. We use dislocation modeling based on contemporary GPS velocities to approximate how shear strain is partitioned among faults at the northern termination of the San Andreas transform system.

GPS velocities are derived from the combination of 1999–2002 observations with initial observations at benchmarks of the California High Precision Geodetic Network (HPGN) established in 1991 by the California Department of Transportation (CalTrans) and the National Geodetic Survey (NGS). Observations utilized in solutions include those of CalTrans (1993, 1994, and 1998), NGS (1994, 1998), Freymueller et al. (1999), Poland et al. (1999), and J. Svarc, (U.S. Geological Survey (USGS), Menlo Park, written communication, 2001). GPS-derived velocity solutions (1993–2002) utilize 66 sites (Table 1) and are presented with respect to a fixed North American plate reference frame (Sella et al., 2002). All sites in Table 1 span at least 2 yrs from initial to final measurement and most sites span at least 8 yrs from initial to final measurement.

Previous USGS geodolite and GPS baseline measurements indicate a transition from ~25 mm/yr of right-lateral shear south of Cape Mendocino to ~15 mm/yr of northeast directed uniaxial contraction north of Cape Mendocino (Murray et al., 1996; Murray and Lisowski, 2000). The USGS has determined coseismic surface displacements from GPS measurements
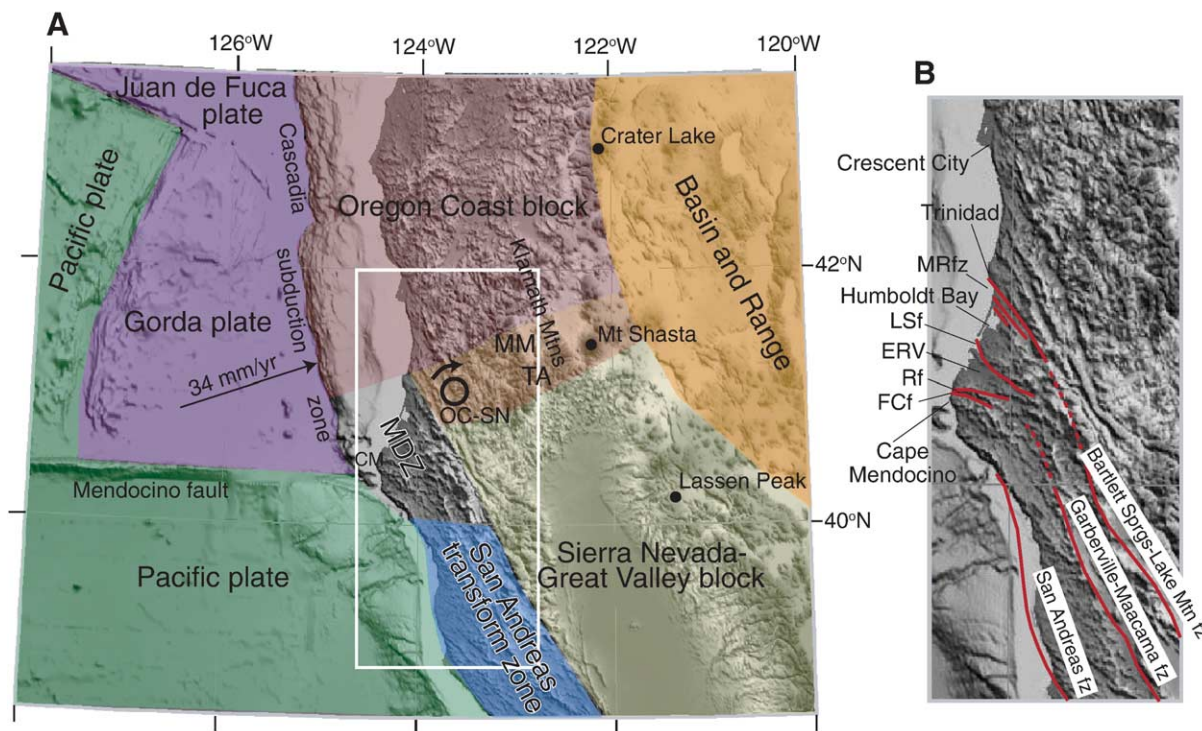

Fig. 1. (A) Plate and block model for region surrounding the Mendocino deformation zone (MDZ). Boundaries of blocks and plates taken after Wells et al. (1998) and Wang et al. (2003). OC–SN, pole of rotation between Oregon Coast block and Sierra Nevada–Great Valley block after Wang et al. (2003). MM, Marble Mountains; TA, Trinity Alps. The region of distinct shading that includes MM, TA and the OC–SN pole is the diffuse boundary zone between the Oregon Coast block and the Sierra Nevada–Great Valley block. The three volcanic centers (Lassen, Shasta, Crater Lake) delineate the approximate location and trend of the Cascade volcanic arc. CM, Cape Mendocino. (B) Map of northernmost coastal California showing the major fault zones and localities discussed in the text. Locations of faults from Kelsey and Carver (1988). MRfz, Mad River fault zone; LSf, Little Salmon fault; ERV, Eel River valley; Rf, Russ fault; FCf, False Cape fault.

Table 1
GPS station velocities relative to a fixed North American plate

Station ID	Longitude (°W)	Latitude (°N)	East velocity (cm/yr)	North velocity (cm/yr)	Sigma E (cm/yr)	Sigma N (cm/yr)	Correlation, east–north
0104	123.2010	39.7954	−1.19	0.86	0.07	0.05	−0.2025
0105	123.8352	39.7769	−2.44	2.66	0.07	0.05	−0.2321
0106	123.5235	40.4602	−0.62	0.85	0.08	0.05	−0.2539
0108	123.4935	40.8153	−0.42	0.91	0.09	0.07	−0.2877
0109	124.1174	40.9750	0.36	1.56	0.10	0.07	−0.3057
0110	123.4759	41.4002	−0.29	0.82	0.17	0.12	0.0245
0113	124.1584	41.9325	0.26	1.07	0.30	0.20	−0.3939
0201	123.1930	41.8415	−0.16	0.99	0.22	0.17	0.1056
0202	122.5913	41.9558	−0.26	0.47	0.26	0.20	0.2065
0208	122.2750	41.5321	−0.20	0.62	0.17	0.11	−0.2194
0212	122.4349	40.9571	−0.74	0.56	0.34	0.15	−0.2760
0217	122.9419	40.6521	−0.63	0.74	0.09	0.07	−0.0859
0220	120.3665	40.7992	−0.44	0.45	0.18	0.09	−0.0423
0221	122.9364	40.3696	−0.82	0.62	0.09	0.06	−0.0755
0226	119.9944	40.2450	−0.53	0.53	0.17	0.09	−0.0467
0229	122.5768	40.6476	−1.13	0.48	0.26	0.17	−0.3554
0411	123.0381	38.3240	−2.00	3.17	0.18	0.11	−0.0852
0412	122.4068	38.4411	−1.01	1.53	0.16	0.09	0.0787
0413	123.4008	38.6533	−2.47	3.41	0.12	0.07	−0.0568
0414	122.8121	38.6709	−1.15	2.33	0.14	0.08	−0.0395
1005	120.2667	37.9972	−1.06	0.35	0.28	0.11	−0.0966
1402	123.9852	40.8876	0.23	1.33	0.24	0.13	−0.2162
1436	123.7905	39.6691	−2.08	2.67	0.31	0.12	0.0590
1468	124.1557	40.4481	−0.66	2.47	0.16	0.07	0.0184
8767	124.2176	40.7669	0.60	1.94	0.14	0.09	−0.1297
9750	124.1815	41.7484	0.11	1.01	0.20	0.13	−0.1112
01KD	123.7945	40.0942	−1.59	2.03	0.19	0.08	0.0472
01LD	123.8316	40.2508	−1.26	1.77	0.19	0.08	0.0528
01MC	123.9211	40.3225	−1.09	1.94	0.20	0.08	0.1092
01NC	124.0330	40.4396	−0.53	2.07	0.20	0.09	0.0300
01ND	123.7974	40.4721	−0.28	1.57	0.22	0.16	0.1096
01NE	123.6751	40.4390	−0.80	1.41	0.18	0.06	0.0722
01PA	124.2556	40.5890	0.00	2.18	0.15	0.09	0.0087
01PB	124.2034	40.6393	0.29	1.95	0.28	0.15	−0.3681
01QB	124.1994	40.7447	0.03	1.91	0.26	0.14	−0.3290
01QF	123.3251	40.8145	−0.41	0.57	0.16	0.09	−0.1372
01RB	124.0874	40.9065	0.15	1.59	0.23	0.14	−0.0694
01RD	123.7724	40.8964	−0.50	0.98	0.14	0.07	−0.2192
01RE	123.6225	40.9439	−0.60	0.99	0.12	0.07	−0.1262
ALEN	124.0951	41.1917	0.40	1.17	0.16	0.11	0.1622
ALGO	78.0714	45.9558	−0.04	0.03	0.05	0.03	0.0544
ANDE	122.2906	40.4195	−1.05	0.74	0.21	0.14	−0.0411
BLDK	123.8654	40.8820	−0.34	1.37	0.13	0.08	−0.0053
BRR2	124.2945	40.4977	−0.68	2.58	0.26	0.08	0.0296
CABL	124.5633	42.8361	0.71	1.33	0.04	0.03	−0.0262
CME1	124.3963	40.4418	−0.61	3.05	0.04	0.03	0.0090
GOL2	116.8893	35.4252	−0.72	0.58	0.04	0.03	0.0423
GOLD	116.8893	35.4252	−0.68	0.57	0.04	0.03	0.0405
GREN	122.5259	41.5550	−0.32	0.36	0.17	0.12	−0.0715
HATC	121.4713	40.8177	−0.63	0.46	0.14	0.10	−0.3177
HOPB	123.0747	38.9952	−1.82	2.11	0.04	0.03	0.0237
KNEE	123.9748	40.7266	0.13	1.44	0.12	0.08	−0.5126
MUMB	122.5326	41.1844	−0.47	0.65	0.07	0.05	−0.0119
NEW2	117.5089	39.6856	−0.20	0.06	0.04	0.04	0.0107
NLIB	91.5749	41.7716	−0.03	0.06	0.04	0.03	0.0270
PENT	119.6250	49.3226	0.20	0.03	0.04	0.04	−0.0872

Table 1 (*continued*)

Station ID	Longitude (°W)	Latitude (°N)	East velocity (cm/yr)	North velocity (cm/yr)	Sigma E (cm/yr)	Sigma N (cm/yr)	Correlation, east–north
PILG	121.9819	41.2597	− 0.68	0.57	0.17	0.11	0.0185
PTRB	123.0187	37.9962	− 2.40	3.56	0.07	0.05	0.0234
PTSG	124.2552	41.7827	0.40	1.14	0.05	0.04	− 0.0050
QUIN	120.9444	39.9746	− 0.76	0.69	0.04	0.03	0.0064
SAGE	120.0388	39.7909	− 0.59	0.27	0.13	0.09	− 0.0713
SHIN	120.2250	40.5917	− 0.46	0.42	0.04	0.03	0.00321
SHLD	119.0157	41.8684	− 0.27	0.21	0.04	0.04	− 0.0063
SUTB	121.8206	39.2058	− 0.95	0.66	0.04	0.03	0.0205
TRND	124.1509	41.0539	0.52	1.64	0.05	0.04	0.0017
YBHB	122.7107	41.7317	− 0.12	0.65	0.04	0.03	− 0.0152

that span the 1992 M_s 7.1 Petrolia, CA earthquake (Oppenheimer et al., 1993; Murray et al., 1996) as well as the offshore 1994 M_w 7.0 Mendocino fault earthquake (Dengler et al., 1995). The USGS Mendocino GPS network spans the MTJ region and is complementary to this study (http://quake.wr.usgs.gov/research/deformation/gps/auto/Mendocino/).

2. Data analysis

GPS phase and pseudorange data were processed using the GIPSY/OASIS II software (Zumberge et al., 1997) following procedures of Freymueller et al. (1999, 2000). For pre-1995 data, global solutions were used to estimate satellite orbits, station coordinates, and nuisance parameters including phase ambiguities and tropospheric path delays. Pre-1995 solutions are those of Freymueller et al. (1999), which are reprocessed to add newly available data. Post-1995 solutions use the Jet Propulsion Laboratory non-fiducial orbits (Zumberge et al., 1997), and include a subset of the available continuous stations that span NA.

Solutions are transformed into the International Terrestrial Reference Frame (ITRF97) (Boucher et al., 1999) evaluated at the epoch of the solution. Each solution contains continuous stations with precise positions and velocities in the ITRF. Each such station is weighted in the estimation of the daily reference frame transformation by the combined uncertainty of its ITRF position and the daily solution. After transformation, three-dimensional root mean square position agreement with ITRF97 is typically ~6 mm. The transformed solutions are used to derive velocities of each station in the ITRF97 frame. Observed coseismic displacements of the 1994 Mendocino fault earthquake sequence (Dengler et al., 1995; M.H. Murray, 2000, written communication) were used to interpolate displacement values for HPGN stations without immediate post-earthquake surveys (Williams, 2002). Displace-

ments were then used to correct pre-earthquake surveys used in the velocity solution.

Velocities relative to NA use a global GPS-only defined plate model, REVEL-2000 (Sella et al., 2002), which gives the motion of the plates in ITRF97. Average station velocity uncertainties are ~2 mm/yr, including the uncertainty in defining the North American frame.

3. Observations

Northern California GPS station velocities are characteristic of a broadly deforming plate boundary zone (Fig. 2A; Table 1). The northern Sierra Nevada–Great Valley (SNGV) sites are moving 10.8 ± 0.5 mm/yr northwest (QUIN and SUTB; Fig. 2A), consistent with other GPS solutions that span larger portions of the northern SNGV region (10.7 ± 0.4 mm/yr; Prescott et al., 2001). These two northern SNGV sites move northwest ~3 mm/yr more slowly than the rigid block motion model prediction of Dixon et al. (2000); however, the majority of the sites used by Dixon et al. (2000) are located in the southern part of the SNGV block. Sites in the eastern Klamath Mountains (7.1 ± 1.1 mm/yr) and the southernmost western Cascade volcanic arc (9.7 ± 1.9 mm/yr) display northwest-directed motion, and sites further north move due north (Figs. 2A and 3A).

North of Cape Mendocino, inland stations converge upon coastal stations (Fig. 3A). Inland stations as close as ~50 km to the coast are moving ~10–12 mm/yr to the northwest, sub-parallel to northern SNGV block motion. The region separating inland northwest-directed velocities from coastal northeast-directed velocities marks the boundary between subduction-dominated interseismic strain at the coast and translational strain of the interior southern Klamath Mountains, where the Klamath Mountains (Fig. 1) are at the northwest end of the P–NA velocity field (Miller et al., 2001; Wells and Simpson, 2001). Inland and north of Cape Mendocino,
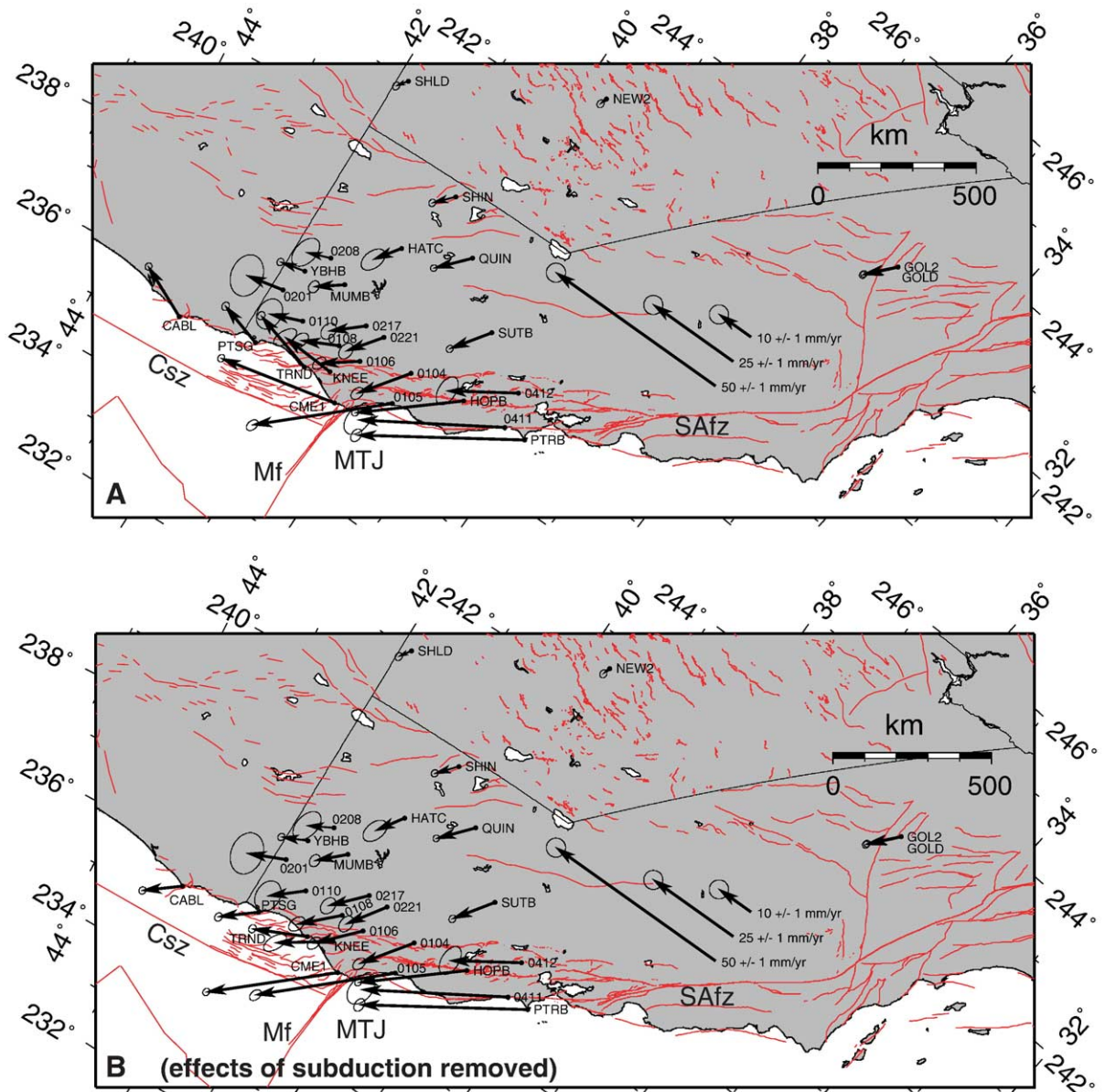
Fig. 2. (A) Oblique Mercator projection about a pole of rotation determined for observed P–NA relative plate motion (Sella et al., 2002) with base of figure parallel to P–NA relative motion. GPS station velocities (1993–2002) are shown relative to the NA plate (Sella et al., 2002). Uncertainty ellipses at velocity vector tips show 2σ (95%) confidence regions. Red lines are mapped faults (Jennings, 1994). Mf, Mendocino fault; MTJ, Mendocino triple junction; SAfz, San Andreas fault zone; Csz, Cascadia subduction zone. (B) Residual velocities after subtracting the modeled interseismic strain accumulation on the southern Csz.

the Mad River fault zone (MRfz, Figs. 1 and 4) and the Lake Mountain fault zone (BS/LMfz; Figs. 1 and 4) occur at the western edges of the Klamath Mountains and SNGV blocks, respectively.

Stations at and near Cape Mendocino are uniformly moving ~N10°W (sub-parallel to the trend of the southern CSZ trench), whereas coastal stations north of Trinidad, CA (TRND) are uniformly moving ~N20–

30°E (sub-parallel to Gorda–NA convergence) (Fig. 3A). Northeast directed station velocities north of Cape Mendocino (CME1; 31.1 ± 0.5 mm/yr) decrease rapidly northward to 17.2 ± 0.6 mm/yr at Trinidad (TRND) and 12.1 ± 0.6 mm/yr at Crescent City, CA (PTSG) (Fig. 3A).

Station velocities inland of Cape Mendocino increase westward across the northernmost SAF system (0106 to
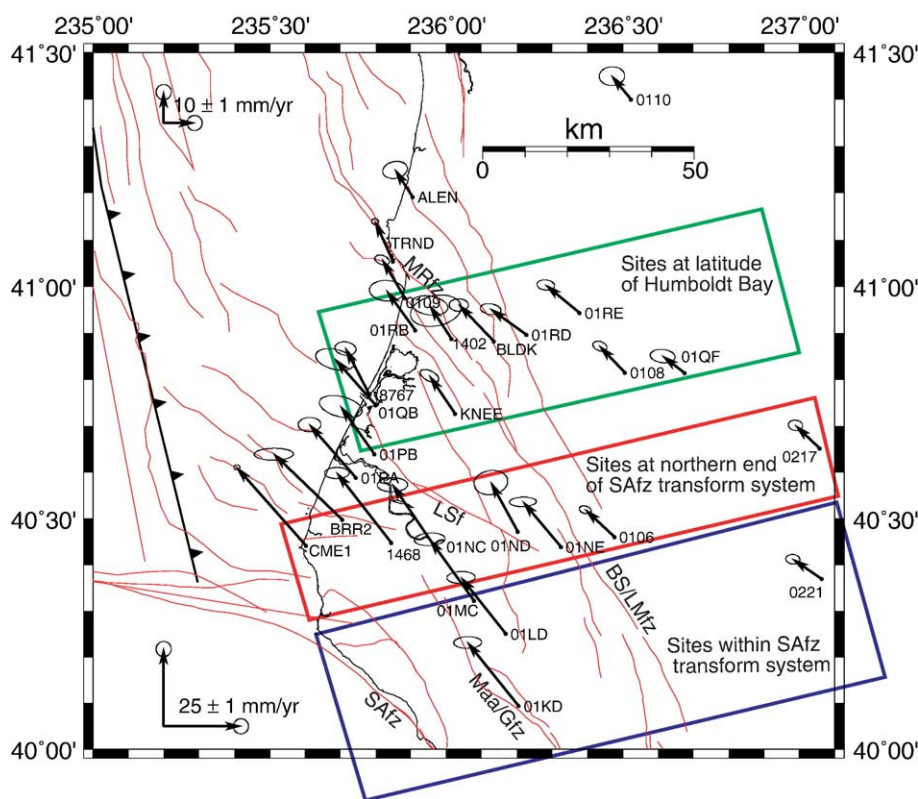
Fig. 3. (A) Observed GPS station velocities (1993–2002). (B) Residual velocities after subtracting the modeled interseismic strain accumulation on the southern Csz; barbed fault represents modeled subduction fault of Flück et al. (1997). Same map projection as Fig. 2.

CME1; Fig. 3A). Distributed relative motion of 22.0 ± 1.1 mm/yr occurs inland from Cape Mendocino across an ~80 km-wide region (Fig. 3A). This is approximately half the Pacific–SNGV relative plate motion observed in the coast ranges ~120 km south of Cape Mendocino (40–41 mm/yr; Freymueller et al., 1999).

4. Correction for the locked subduction zone

Strain resulting from the locked CSZ offshore contributes a component of the velocity field for all sites near the coast. This elastic deformation produces contraction in the direction of relative motion between the

Fig. 4. Distributed deformation related to northward migration of the Mendocino triple junction, based on GPS residual velocities (velocities with subduction signal removed). Red lines are mapped faults (Jennings, 1994). Barbed fault represents southern Cascadia subduction zone. The three rectangles (green, red and blue) enclose the green, red and blue GPS stations depicted on the profiles in Fig. 5. LSf, Little Salmon fault; MRfz, Mad River fault zone; SAfz, San Andreas fault zone; Maa/Gfz, Maacama/Garberville fault zone; BS/Lmfz, Bartlett Springs/Lake Mountain fault zone.

subducting plate and overriding plate. Sites near the coast move most rapidly in the direction of relative plate motion, with sites far inland being unaffected. Additional complexities result if there are significant along-strike variations in plate coupling near the MTJ where the subduction zone ends. The exact contribution of the locked subduction zone to the velocity field depends on the orientation of plate convergence between the downgoing plate and forearc, the width of the locked zone, and the width of the transition zone from fully locked to fully creeping at the base of the locked zone.

To evaluate other tectonic signals independently from subduction, we use a dislocation model modified from Flück et al. (1997) to calculate, and then remove, the component of interseismic strain caused by the locked CSZ. The dislocation model incorporates a fully locked zone 50 km wide and a transition zone from locked to creeping of the same width (Flück et al., 1997). For comparison, an earlier model developed by Verdonck (1995) utilized a locked zone of 75 km and a transition zone of 125 km. The plate convergence rate

and direction depends on the assumed motion of the forearc relative to North America (e.g., Wang et al., 2003).

Because the transition between the SNGV block in the south and the Oregon Coast forearc block in the north occurs near the Mendocino deformation zone (Fig. 1), the appropriate convergence rate and direction may vary from south to north across the study area. Miller et al. (2001) derived a Juan de Fuca–North America pole of rotation by combining the DeMets and Dixon (1999) Pacific–North America pole with the alternate Pacific–Juan de Fuca pole of Wilson (1993). Wells and Simpson (2001) determined a new Juan de Fuca–Oregon Coast forearc pole (also reported in Wang et al., 2003), which included the motion of the Oregon Coast relative to North America. In the southernmost part of the study area, the Juan de Fuca–Sierra Nevada relative motion may be more appropriate to drive the dislocation model, but the Juan de Fuca–Sierra Nevada relative velocity near Cape Mendocino is almost identical to the Juan de Fuca–Oregon Coast velocity (SNGV–Oregon Coast relative velocity is no

more than ~10% of the subducting plate velocity at this location).

Wells and Simpson's (2001) pole predicts a relative convergence rate of 34 mm/yr toward 72° in our study area (Fig. 1). This convergence vector results in a maximum model site velocity of 17 mm/yr at Cape Mendocino. Farther north, velocities along the coast are ~10 mm/yr, with the change resulting from the fact that at Cape Mendocino the land protrudes farther west and thus closer to the trench than the northernmost California coastline. Model velocities drop off smoothly but rapidly with distance from the coast, reaching 1–2 mm/yr at the Great Valley or Mt. Shasta area.

The residual velocities (Figs. 2B and 3B), computed by subtracting the modeled interseismic velocities from the observed velocities, represent permanent deformation of the overriding plate and include deformation from upper plate faults, the SAF system and the influence of the SNGV block, as well as errors in the subduction model and measurement error. Residual velocities far inland are the same as the observed GPS velocities (Fig. 3A vs. B) because far field stations are unaffected by interseismic strain above the locked subduction zone. Rates of deformation discussed in the following sections are derived from the residual velocity field, which has removed the influence of the southern CSZ.

The main uncertainty in the subduction correction results from possible variations in the width of the locked and transition zones. We use widths estimated from thermal models and extrapolated from elsewhere in Cascadia (Flück et al., 1997; Wang et al., 2003), but along-strike variations in this width are reported both in Cascadia (e.g., McCaffrey, 2002) and elsewhere (e.g., Zweck et al., 2002). The distribution of slip in the transition zone can also have a measurable impact on the model vectors (Wang et al., 2003). In addition, repeated slow slip events (ETS, Episodic Tremor and Slip) have been identified along the southern Cascadia margin (at site YBHB, Fig. 2) (Szeliga et al., 2004). These events show that the width of these zones is not constant in time. Our site velocities are all averaged over a few years to a decade, or several cycles of ETS. The appropriate locked and transition zone width in this case represent the part of the subduction interface that remains fully or partially locked even in the ETS events.

We ran models using a wider or narrower locked zone, in order to evaluate the potential impact on the residual velocities from errors in the assumed subduction model. In general, the model corrections will be smaller if the locked zone is narrower than we as-

sumed, and larger if the locked zone is wider than we assumed. The differences in model predictions are largest near the coast and drop off rapidly with distance inland. For sites in the central valley of California, or at a similar distance inland to the north, the subduction strain model predicts velocities of 1–2 mm/yr for all models evaluated, with the differences between model predictions being on the order of 0.5 mm/yr. In contrast, model predictions for coastal sites can vary by up to 2–3 mm/yr. In all cases, the differences between predictions of different models were spatially smooth, so errors in the model will not introduce fictitious short-wavelength contractional features into the residual velocity field. This is to be expected, given that the differences in the models result from changes in the deformation source at a depth of ~25–30 km, and deep deformation sources always produce long-wavelength features in the velocity field.

5. Discussion

5.1. Forearc block motions

Residual velocities of sites on the northern SNGV block move both northward and westward, with a significant component of motion toward the coast (SHIN, QUIN, SUTB, HATC; Fig. 2B). Sites further north lack this westward component of motion (YBHB, 0201; Fig. 2B); their residual velocities are nearly parallel to the coast. The residual velocities of the northern sites are compatible with site velocities determined in Oregon (McCaffrey et al., 2000; McCaffrey, 2002) once the effect of subduction is removed, and agree with predicted motion of the Oregon Coast (OC) block (Wells et al., 1998; Wells and Simpson, 2001; McCaffrey, 2002).

The transition between SNGV block velocities and OC block velocities occurs over a ~100-km-wide zone with its southern boundary at roughly the latitude of Cape Mendocino. Inland, the transition is seen clearly between sites HATC, with SNGV-directed motion, and YBHB and 0208, with OC-directed motion (Fig. 2B). Near the coast, the exact location of the transition is less clear due to uncertainties in the subduction correction, but moving northward a progressive clockwise rotation of the velocity vectors can be seen, for example comparing sites 0104, 0106 and 0108 (Fig. 3B). Although the relative motion between the SNGV and OC forearc blocks is small at their boundary, the SNGV block rotates anti-clockwise relative to North America, while the OC block rotates clockwise (Wells et al., 1998; Wells and Simpson, 2001). The angular veloci-

ties of these two blocks seem to be ideal to minimize the relative motion at their boundary, and the motion of these two blocks opens space on their trailing edges to accommodate Basin and Range extension. The glaciated Marble Mountains and Trinity Alps (MM, TA; Fig. 1) comprise the highest topography in the region and are located within the boundary zone between these two blocks. This boundary zone may be diffuse (Fig. 1), but relative motions are too small and GPS sites too sparse at this point to resolve whether one or several active faults takes up the difference in forearc block motions between the OC and SNGV blocks.

5.2. Cape Mendocino and the northern San Andreas fault system

In northern California, residual velocities are sub-parallel to the SAF system and related SNGV block motion, reflecting the influence of the P–NA plate boundary on the southern CSZ (Fig. 2B). Slivers of crust between the faults of the northern SAF system move in a right-lateral sense relative to the SNGV block at least as far as Cape Mendocino (0411, HOPB, 0412; Fig. 2B). Continuous station CME1 located above Cape Mendocino is moving 33.8 ± 0.5 mm/yr sub-parallel to P–NA relative motion (Figs. 2B and 4). Although the extension of the San Andreas fault itself is offshore at this latitude, elastic strain from the locked SAF will contribute to this velocity. The distributed right-lateral motion between Cape Mendocino (33.8 ± 0.5 mm/yr) and station 0106 (13.9 ± 1.1 mm/yr) (Fig. 4) is ~34% of the total P–SNGV relative motion observed in the coast ranges ~120 km south of Cape Mendocino (Freymueller et al., 1999). The westward increases in velocity that span stations 0106 and CME1 (Figs. 3B and 4)

are consistent with right-lateral strain on mapped north–northwest-trending faults (Fig. 4), the Bartlett Springs–Lake Mountain fault zone (BS/LMfz) to the east, the Maacama–Garberville fault zone (Maa/Gfz), and the offshore San Andreas fault zone (Fig. 4) (Kelsey and Carver, 1988).

Right-lateral shear strain is seen in the residual velocity field at the latitude of Cape Mendocino (red rectangle, Fig. 4). Because the offshore San Andreas fault terminates to the south of the latitude of Cape Mendocino, right-lateral shear strain must result from onshore faults, or distributed shear. Distinct strike–slip faults reaching the surface with Holocene scarps have not been found on either the Maa/Gfz or the BS/LMfz north of approximately 40°N; therefore, the right-lateral shear strain on north of 40°N probably involves distributed shear.

Although right-lateral shear strain is expected because strike–slip faults of the SAF system must propagate northward as the MTJ propagates northward (Dickinson and Snyder, 1979), residual velocities show reduced right-lateral shear strain at the latitude of Humboldt Bay (~40.75°N, green rectangle, Fig. 4). Therefore, the northern end of the shear strain associated with the SA transform boundary, as reflected in the residual velocities, is north of the latitude of Cape Mendocino and appears to be at the latitude of Humboldt Bay.

We make a more quantitative comparison among sites with SAF-parallel residual velocities at the northern end of the SAF transform system by projecting the SAF-parallel velocities of Fig. 4 onto a profile that strikes 57°, perpendicular to the average SAF system strike at 40°N, and constructing 2D elastic models (Table 2 and Fig. 5). We divided the sites into three latitudinal swaths, sites at the latitude of Humboldt Bay

Table 2
2D elastic models for the faults of the San Andreas fault system

Model	San Andreas fault zone, rate (mm/yr)	San Andreas fault zone, locking depth (km)	Maacama/Garberville fault zone, rate (mm/yr)	Maacama/Garberville fault zone, locking depth (km)	Bartlett Springs/Lake Mountain fault zone, rate (mm/yr)	Bartlett Springs/Lake Mountain fault zone, locking depth (km)
Model for San Andreas transform from Freymueller et al. (1999), (dashed blue profile, Fig. 5)[a]	17	15	14	13	8	0
Model for northern end of San Andreas transform (blue profile, Fig. 5)[b]	17	15	14	13	8	5
Sites at latitude of Humboldt Bay (north of MTJ) (green profile, Fig. 5)[c]	0	0	0	0	8	13

[a] Model constructed from sites at latitudes 39° to 39.5°N, ~100–120 km south of Cape Mendocino (Freymueller et al., 1999).
[b] Model constructed from sites within blue and red rectangles of Fig. 4.
[c] Model constructed from sites within green rectangle of Fig. 4.
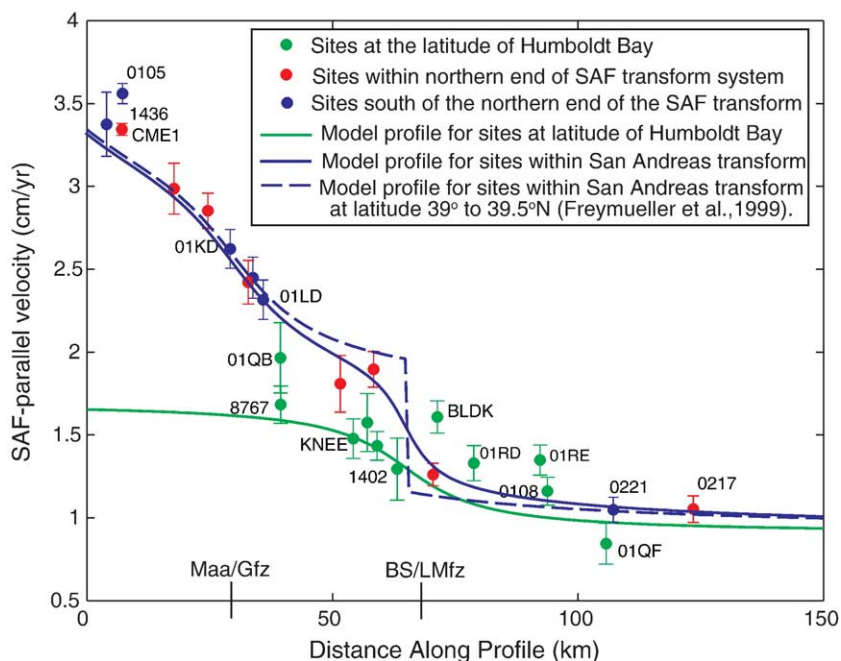
Fig. 5. Three velocity profiles from three fault dislocation models perpendicular to trend of San Andreas fault plate boundary (see Table 2 for model parameters). Distributed strike–slip motion occurs across the two eastern strands of the San Andreas fault system, with velocity increases near surface traces of the Maacama/Garberville fault zone (Maa/Gfz) and the Bartlett Springs/Lake Mountain fault zone (BS/LMfz). The (arbitrary) origin of the profiles is near Punta Gorda, the Maa/Gfz is at 30 km distance, and the BS/LMfz is at 65 km distance. The model curves are based on trial and error fits to their respective data. The green model curve is fit to the green stations (those within the green rectangle, Fig. 4), and the blue model curve is fit to the blue and red stations (those within the blue and red rectangles, Fig. 4). The dashed blue model curve (from Freymueller et al., 1999), which is identical to the blue curve except that the BS/LMfz is creeping at the surface, is the velocity profile across the San Andreas fault system ~120 km further south at latitude range 39° to 39.5°N.

(green rectangle, Fig. 4), sites within the northern end of the San Andreas transform at the latitude of Cape Mendocino (red rectangle, Fig. 4), and sites south of the northern end of the San Andreas transform (blue rectangle, Fig. 4). Because our velocities are referenced to NA, we must include the motion of SNGV relative to NA, plus each of the faults of the SAF system. The uncertainty in SNGV–NA motion is a few mm/yr in all existing plate/block motion models (e.g., Sella et al., 2002), so we used the motion of the site QUIN in the Sierra Nevada (9 mm/yr right-lateral normal to the profile) as the motion of SNGV. For fault location, we recognize that the faults generally show an eastward dip (Castillo and Ellsworth, 1993) and there is an uncertainty of a few km in the fault locations at depth, but our model results are only weakly sensitive to the exact locations of the faults as long as every site is on the correct side of the closest fault.

For those sites within the San Andreas transform system (within the red and blue rectangles, Fig. 4), our modeling results in Fig. 5 show no significant along-strike changes in the San Andreas fault-parallel velocities at the latitude of 40° to 40.5°N (red and blue sites

both fit with solid blue profile line, Fig. 5) compared to San Andreas fault-parallel velocities at the latitude of 39° to 39.5°N (dashed blue profile line, Fig. 5). The dashed blue profile (Fig. 5) is a velocity model developed by Freymueller et al. (1999) for a transect of ~120 km to the south (best-fitting fault slip rates and locking depths tabulated in Table 2) and does an excellent job of fitting most of the data from the northern part of the transform system with the exception that the locking depth of the eastern most fault has been adjusted because the BS/LMfz shows evidence of shallow creep to the south at 39.5°N whereas evidence of creep is lacking on the BS/LMfz in the latitude range 40° to 40.5°N (Fig. 5). The velocities of the westernmost sites are slightly underpredicted, and the fit could be improved by decreasing the slip rate of the SAfz slightly and increasing the slip rate of the Maa/Gfz correspondingly.

Sites in the northern latitudinal swath through Humboldt Bay (green station velocities, Fig. 5), a region that is north of the northern end of the San Andreas transform, show a different pattern of SAF-parallel velocities from those further south. SAF-parallel velocities are

similar to sites further south in the eastern part of the area (eastern part of green rectangle) but sites in the western part of the area have progressively faster SAF-parallel velocities, although not as fast as sites to the south–southeast along strike. No simple model involving only known active faults explain the data from this profile well. We show a model in which the BS/LMfz continues northward with the same slip rate as in the southern profile (8 mm/yr), but with a locking depth of 12 km (Fig. 5 and Table 2). Although such a fault model explains about half of the data well, it under-predicts the velocities of the other half of the sites (Fig. 5). In addition, a component of right-lateral shear is observed extending much farther to the east than in the southern profiles (note the clear difference in velocity between sites 0108 and 01QF (Fig. 4) and the jump in velocity from ~0.8 cm/yr to 1.3 cm/yr at about ~30 km east of the BS/LMfz (green site velocities, Fig. 5)). This component of right-lateral shear occurs in an area where there is no known active Quaternary fault.

We infer that the SAF-parallel residual velocities at the latitude of Humboldt Bay (green rectangle, Fig. 4) are a product of both Gorda–NA plate interaction and Pacific–NA interaction. The right-lateral shear strain evident at the latitude of Humboldt Bay reflects right-lateral shear propagating north–northwestward on the BS/LMfz (Pacific–NA interaction) as depicted by the model (Fig. 5). However, the origin of the SAF-parallel velocities to the north of the latitude of Cape Mendocino, which is not predicted by a right slip model that stops at the latitude pf Cape Mendocino (south edge of the Gorda plate), may be the viscous coupling of the Gorda plate to the North America (NA) plate through the slab window (Furlong and Govers, 1999). Although we subtracted out the subduction zone component (subduction interface coupling) from these SAF-parallel velocities, we did not subtract out the interplay of Gorda–NA in the slab window region where upper mantle and lower crust is coupled viscously to both the southern edge of the Gorda slab and the overlying NA plate, thereby dragging NA northward (Furlong and Govers, 1999). The viscous drag produces the northward residual velocities of ~0.3 to 0.8 cm/yr, accounting for the additional velocity not predicted by the right slip fault model.

5.3. Pacific–North America margin-parallel contraction

The transition from predominately translational strike–slip to predominately convergent subduction tectonics occurs over a ~80 km distance from the Eel River mouth (near 01 PA) to Trinidad, CA (TRND), where station velocities indicate SAF-parallel shortening. The northwest–southeast (SAF-parallel) shortening occurs at the tips of the northern SAF fault system (Figs. 1B and 4) and is a consequence of the rapid decrease in residual station velocities immediately north of Cape Mendocino, a region coincident with the southern edge of the subducted Gorda plate (Smith et al., 1993). Average northwest–southeast shortening among three pairs of sites at the latitude of Cape Mendocino (1468-01PA, 01NC-01PB, and 01NE-KNEE; Fig. 4) is ~8.0 ± 2.0 mm/yr. Similarly, there is ~9.0 ± 5.0 mm/yr of SAF-parallel shortening between the Trinidad area (stations ALEN and TRND) and stations inland of Cape Mendocino (stations 01ND and 01NE, Fig. 4). This SAF-parallel shortening is essentially orthogonal to the strain direction predicted from the subduction strain model and is not affected by variation in the width of the locked zone nor variations in the assumed convergence direction of up to ~30°. The SAF-parallel shortening cannot be explained as a result of elastic deformation from the locked offshore SAF, because the SAF does not extend this far north.

SAF-parallel shortening north of the latitude of the MTJ may result from two processes, crustal slivers within the eastern SAF system impinging northward on the SNGV and OC forearc blocks as the SAF system propagates northward and viscous coupling of the NA plate (SNGV block) to the underlying south edge of the Gorda slab. In the first instance, rapid velocities west of the Maa/Gfz from the south impinge on slower velocities along strike to the north in the Humboldt Bay region (Figs. 4 and 5), producing SAF-parallel shortening west and north of the north–northwest extension of the Maa/Gfz. In the second instance, shortening is the product of bulk strain associated with the Mendocino crustal conveyor, whereby lower crust and upper mantle viscous coupling within the slab window at the south edge of the subducted Gorda plate drives north–south shortening in the North American plate above the southern edge of the subducted plate (Furlong and Govers, 1999; Furlong et al., 2003).

SAF-parallel shortening in the MTJ region is accommodated as permanent strain on several sets of mapped structures in the general latitude of the Eel River valley and Humboldt Bay area north of Cape Mendocino. Faults accommodating SAF-parallel contraction include the high-angle reverse faults immediately north of Cape Mendocino (Russ fault and False Cape fault; Rf and FCf, Fig. 1) and the active upper plate thrust faults of Mad River fault zone and Little Salmon fault (MRfz and LSf, Fig. 1) (Ogle, 1953; McLaughlin et al., 2000),

where contraction would be accommodated by oblique reverse motion. Folds accommodating SAF-parallel contraction include the long wavelength (~10 km), east–west trending folds apparent both in the margins of the Eel River valley (ERV, Fig. 1) (Ogle, 1953) and in the marine terraced upland near station TRND (Trinidad, Fig. 1) (McCrory, 2000).

5.4. Convergence of Sierra Nevada–Great Valley block with the coast

Stations in the northern SNGV block greater than 100 km inland of the SAF display velocities oriented slightly westward of the P–NA relative motion direction (Fig. 3B; long axis of Fig. 3B is parallel to P–NA relative motion direction). Convergence of SNGV block motion with the MTJ region results in a zone of contraction that begins ~130 km east of the coast near station 0217 near Weaverville, CA (Figs. 2 and 4) and persists westward towards the Humboldt Bay region. The western edge of this contraction is within the MRfz to the north of Humboldt Bay and further south the edge is just west of the BS/LMfz (note converging GPS-derived velocities across these fault zones, 01RD to 1402 across the MRfz and 0106 to 01NE across the BS/LMfz, Fig. 4). Similarly, near the San Francisco Bay area >300 km south, the SNGV block is converging at ~2–4 mm/yr with the eastern SAF system (Prescott et al., 2001). The contraction between the interior of the SNGV and the coast appears to require contraction on structures both at the western edge of the Great Valley (east of station 0217, Fig. 2) and on fault zones near the coast such as the Mad River fault zone. Although the residual velocity field shows zones of concentrated contraction corresponding to the upper crustal fault zones, errors in the subduction strain model might result in more broadly distributed contraction. Better resolution of the details will require both more precise velocities and greater site density, and also further constraints on the subduction strain model.

6. Conclusions

Although characterized as a triple junction region on the basis of simple plate boundary geometry, we show on the basis of GPS station velocities that the north coastal California area is more accurately depicted as a quadruple junction of four blocks, the Mendocino deformation zone (MDZ, Fig. 1); the four blocks are the Pacific plate, the Gorda plate, the Sierra Nevada–Great Valley block and the Oregon Coast block (Fig. 1). The San Andreas transform zone is a broad boundary be-

tween the Pacific plate and the western edge of the Sierra Nevada Great Valley block, with the northern end of the transform zone overlying the southern edge of the subducted Gorda plate that is viscously coupled to the overlying western margin of the Sierra Nevada–Great Valley block. The northern end to the Sierra Nevada–Great Valley block bounds the Oregon Coast block; the diffuse boundary between the two blocks occurs inland from Humboldt Bay at the approximate latitude of elevated topography of the Trinity Alps and the Marble Mountains (TA and MM, Fig. 1). The southernmost Gorda plate subducts beneath the upper plate at the latitude of Humboldt Bay. The Humboldt Bay region (the upper plate) is a zone of crustal deformation that is both at the northern end of the San Andreas fault transform system and at the western end of the westward converging Sierra Nevada Great Valley block.

Using GPS station velocities, we depict the pattern of strain among these four crustal blocks in northern California. After removing the component of elastic strain accumulation caused by the Cascadia subduction zone, we infer that observed strain accumulation in the region is a consequence of the northern termination of the San Andreas transform system and the westward convergence of the Sierra Nevada–Great Valley block. Right-lateral shear strain propagates northward of the latitude of Cape Mendocino along the two eastern strands of the San Andreas transform system, the Bartlett Springs/Lake Mountain fault zone and the Garberville/Maacama fault zone (Fig. 1B). Further north at the latitude of Humboldt Bay, San Andreas fault-parallel velocities are less and therefore shortening parallel to the trend the San Andreas fault occurs in the Humboldt Bay region.

The San Andreas fault-parallel shortening is expressed as contractional strain on several major structures in the Humboldt Bay area. San Andreas fault-parallel shortening is accommodated by the east–west-trending folds in the Eel River valley and near Trinidad, by slip on the east–west-trending Russ and related faults east of Cape Mendocino and by oblique slip on the northwest trending Little Salmon fault and the Mad River fault zone (Fig. 1B).

The Sierra Nevada Great Valley block converges toward the coast; based on station velocities, a component of this convergence probably is accommodated at or near the western edge of the northern Sacramento Valley while the westernmost component of convergence may be accommodated by east–west shortening across the Mad River fault zone within 20 km of the coast. Although the active upper plate reverse faults in

the Humboldt Bay region (Little Salmon fault and Mad River fault zone, Fig. 1B) are perpendicular in trend to the Gorda–North America convergence direction, strain on these faults probably has a polygenetic origin, with a converging forearc block on the east, an impinging transform system and viscously coupled slab window to the south and strain associated with a convergent plate boundary to the west.

Acknowledgements

References

Boucher, C., Altamini, Z., Sillard, P., 1999. The 1997 International Terrestrial Reference Frame (ITRF97). IERS Technical Note, vol. 27. Observatoire de Paris, Paris, France.

Castillo, D.A., 1993. Seismotectonics of the San Andreas fault system between point arena and Cape Mendocino in Northern California: implication for the development and evolution of a young transform. Journal of Geophysical Research 98, 6543–6560.

Clarke Jr., S.H., Carver, G.A., 1992. Late Holocene tectonics and paleoseismicity, southern Cascadia subduction zone. Science 255, 188–192.

DeMets, C., Dixon, T.H., 1999. Kinematic models for Pacific–North America motion from 3 Ma to present: I. Evidence for steady state

motion and biases in the NUVEL-1A model. Geophysical Research Letters 26, 1921–1924.

Dengler, L., Moley, K., McPherson, R., Pasyanos, M., Dewey, J.W., Murray, M.H., 1995. The September 1, 1994 Mendocino fault earthquake. California Geology 48, 43–53.

Dickinson, W.R., Snyder, W.S., 1979. Geometry of triple junctions related to San Andreas transform. Journal of Geophysical Research 84, 561–572.

Dixon, T.H., Miller, M.M., Farina, F., Wang, H., Johnson, D.J., 2000. Present-day motion of the Sierra Nevada block and some tectonic implications for the Basin and Range province, North America Cordillera. Tectonics 19, 1–24.

Flück, P., Hyndman, R.D., Wang, K., 1997. Three_dimensional dislocation model for great earthquakes of the Cascadia subduction zone. Journal of Geophysical Research, 102, 20,539–20,550.

Freymueller, J.T., Murray, M.H., Segall, P., Castillo, D., 1999. Kinematics of the Pacific–North America plate boundary zone, northern California. Journal of Geophysical Research 104, 7419–7441.

Freymueller, J.T., Cohen, S.C., Fletcher, H.J., 2000. Spatial variations in present-day deformation, Kenai Peninsula, and their implications. Journal of Geophysical Research 105, 8079–8101.

Furlong, K.P., Govers, R., 1999. Ephemeral crustal thickening at a triple junction: the Mendocino crustal conveyor. Geology 27, 127–130.

Furlong, K.P., Lock, J., Guzofski, C., Whitlock, J., Benz, H., 2003. The Mendocino crustal conveyor: making and breaking the California crust. International Geology Review 45, 767–779.

Jennings, C., 1994. Fault activity map of California and adjacent areas. Department of Conservation, California Division of Mines and Geology, Sacramento, CA.

Kelsey, H.M., Carver, G.A., 1988. Late Neogene and Quaternary tectonics associated with the northward growth of the San Andreas transform fault, northern California. Journal of Geophysical Research 93, 4797–4819.

Lisowski, M., Savage, J.C., Prescott, W.H., 1991. The velocity field along the San Andreas fault in northern California. Seismological Research Letters (abs) 62, 11.

McCaffrey, R., 2002. Crustal block rotations and plate coupling. In: Stein, S., Freymueller, J. (Eds.), Plate Boundary Zones. AGU Geodynamics Ser., vol. 30, pp. 101–122.

McCaffrey, R., Long, M.D., Goldfinger, C., Zwick, P., Nabelek, J., Johnson, C.K., Smith, C., 2000. Rotation and plate locking along the southern Cascadia subduction zone. Geophysical Research Letters 27, 2117–2120.

McCrory, P.A., 2000. Upper plate contraction north of the migrating Mendocino triple junction, northern California: implications for strain partitioning. Tectonics 19, 1144–1160.

McLaughlin, R.J., Ellen, S.D., Blake, M.C., Jayko, A.S., Irwin, W.P., Aalto, K.R., Carver, G.A., Clarke, S.H., 2000. Geology of the Cape Mendocino, Eureka, Garberville and southwestern part of the Hayfork 30 × 60 minute quadrangles and adjacent offshore area, northern California. Miscellaneous Field Studies MF, 2336.

Miller, M.M, Johnson, D.J., Rubin, C.M., Dragert, H., Wang, K., Qamar, A., Goldfinger, C., 2001. GPS-determination of along-strike variation in Cascadia margin kinematics: implications for relative plate motion, subduction zone coupling, and permanent deformation. Tectonics 20, 161–176.

Murray, M.H., Lisowski, M., 2000. Strain accumulation along the Cascadia subduction zone. Geophysical Research Letters 27, 3631–3634.

Murray, M.H., Marshall, G.A., Lisowski, M., Stein, R.S., 1996. The 1992 M=7 Cape Mendocino, California, earthquake: Coseismic deformation at the south end of the Cascadia megathrust. Journal of Geophysical Research 101, 17, 707–17, 725.

Ogle, B.A., 1953. Geology of the Eel River Valley area, Humboldt County, California. California Division of Mines Bulletin 164 (128 pp.).

Poland, M.P., Burgmann, R., Fink, J.H., Dzurisin, D., 1999. Deformation field at Medicine Lake Volcano, Northern California; new results from GPS measurements. EOS, Transactions, American Geophysical Union 80, 960.

Prescott, W.H., Savage, J.C., Svarc, J.L., Manaker, D., 2001. Deformation across the Pacific–North America plate boundary near San Francisco, California. Journal of Geophysical Research 106, 6673–6682.

Oppenheimer, D., et al., 1993. The Cape Mendocino, California, earthquakes of April, 1992: subduction at the triple junction. Science 261, 433–438.

Sella, G.F., Dixon, T.H., Mao, A., Stein, S., 2002. REVEL: a model for Recent plate velocities from space geodesy. Journal of Geophysical Research 107. doi:10.1029/2000JB000033.

Smith, S.W., Knapp, J.S., McPherson, R.C., 1993. Seismicity of the Gorda plate, structure of the continental margin, and an eastward jump of the Mendocino triple junction. Journal of Geophysical Research 98, 8153–8171.

Snay, R.A., Matsikari, T., 1991. Horizontal deformation in the Cascadia subduction zone from serendipitous data. Tectonophysics 94, 59–67.

Szeliga, W., Melbourne, T.I, Miller, M.M., Santillan, V.M., 2004. Southern Cascadia episodic slow earthquakes. Geophysical Research Letters 31, LI6602. doi:10.1029/2004GL020824.

Verdonck, D., 1995. Three dimensional model of vertical deformation at the southern Cascadia subduction zone, western United States. Geology 23, 261–264.

Wang, K., Wells, R., Mazzotti, S., Hyndman, R.D., Sagiya, T., 2003. A revised dislocation model of interseismic deformation of the Cascadia subduction zone. Journal of Geophysical Research 108 (B1), 2026. doi:10.1029/2001JB001227.

Wells, R.E., Weaver, C.S., Blakely, R.J., 1998. Forearc migration in Cascadia and its neotectonic significance. Geology 26, 759–762.

Wells, R.E., Simpson, R.W., 2001. Northward migration of the Cascadia forearc in the northwestern U.S. and implications for subduction deformation. Earth Planets Space 53, 275–283.

Wessel, P., Smith, W.H.F., 1995. New version of the Generic Mapping Tools released. EOS, Transactions, American Geophysical Union 76, 329.

Williams, T.B., 2002. The geodetic signature of modern deformation (1993–2002) within the Southern Cascadia Subduction Zone, northwestern California, MS thesis, Humboldt State University, Arcata. 102 pp.

Wilson, D.S., 1993. Confidence intervals for motion and deformation of the Juan de Fuca plate. Journal of Geophysical Research 98, 16053–16071.

Zumberge, J.F., Heflin, M.B., Jefferson, D.C., Watkins, M.M., Webb, F.H., 1997. Precise point positioning for the efficient and robust analysis of GPS data from large networks. Journal of Geophysical Research 102, 5005–5017.

Zweck, C., Freymueller, J.T., Cohen, S.C., 2002. Elastic dislocation modeling of the postseismic response to the 1964 Alaska Earthquake. Journal of Geophysical Research 107 (B4). doi:10.1029/2001JB000409.